Longitudinal proteomic profiling of T cell differentiation *in vivo* unveils dynamic proteome remodeling

Christian M. Beusch[1,2,3,4,10*], Abdelhameed S. Dawood[1,2*], Ahmet Ozdilek[1,2], Sarah Welbourn[1,2,3,4], Christopher M. Monaco[1,2,3,4,5], Alexandra S. Flegle[1,2,6], Sakshi Malik[2,7,9], Christina Niavi[2,7,8], Akil Akhtar[2,7], Carly Roman[2,7,8], Autumn A. Gavora[2,7], David E. Gordon[1,2,3,4,5 #], and Mohamed S. Abdel-Hakeem[1,2,3,6,8,11 #]

[1] Pathology Advanced Translational Research Unit (PATRU), Department of Pathology and Laboratory Medicine, Emory University School of Medicine, Atlanta, GA, USA

[2] Emory Vaccine Center, Emory University School of Medicine, Atlanta, GA, USA

[3] Winship Cancer Institute, Emory University School of Medicine, Atlanta, GA, USA

[4] Wallace H. Coulter Department of Biomedical Engineering, Emory University and Georgia Institute of Technology

[5] Molecular and Systems Pharmacology Graduate Program, Emory University, Atlanta, GA, USA

[6] Cancer Biology Graduate Program, Emory University, Atlanta, GA, USA

[7] Department of Microbiology and Immunology, Emory University School of Medicine, Atlanta, GA, USA

[8] Immunology and Molecular Pathology Graduate Program, Emory University, Atlanta, GA, USA

[9] Currently: Department of Pediatrics, Emory University School of Medicine, Atlanta, GA, USA

[10] Department of Surgical Sciences, Uppsala University, Uppsala, Sweden

[11] Department of Microbiology and Immunology, Faculty of Pharmacy, Cairo University, Cairo, Egypt

**Equal contribution, #Corresponding authors*

Abstract

T cell differentiation plays a pivotal role in orchestrating immune responses and is crucial for combating infection. Consequently, extensive studies on the cellular, transcriptional, and epigenetic levels have been conducted to deepen our understanding of T cell differentiation. Despite numerous studies revealing disparities between transcriptional and proteomic measurements of the same cells, there has been no direct ex-vivo proteomic profiling of antigen-specific T cell differentiation conducted thus far. In this study, we performed the first longitudinal proteomic profiling of T cell differentiation *in vivo,* utilizing the well-characterized lymphocytic choriomeningitis virus (LCMV) mouse model. We performed *ex-vivo* protein abundance profiling of effector to memory differentiation (T_{EFF}/T_{MEM}) and early to late exhausted T cell (T_{EX}) differentiation following LCMV infection with the acute Armstrong and chronic Clone-13 strains, respectively. Our findings reveal dynamic alterations of the T cell proteome during differentiation that are either common or distinct for acute and chronic infection, recapitulating existing knowledge. Crucially, our proteomic analyses identify significant differences in the abundance of several proteins between cell states that were not previously highlighted through transcriptional profiling. Our study provides a comprehensive proteomics resource of *in vivo* T cell differentiation within an antigen-specific context, complementing existing omics data and elucidating putative proteins with potential diagnostic and therapeutic relevance.

Introduction

T cells are central to the adaptive immune system in combating tumor cells and intracellular pathogens. During acute infection, naive T cells are activated, giving rise to effector cells (T_{EFF}) which perish or differentiate into memory T cells (T_{MEM}) upon clearing the pathogen. This is accompanied by extensive changes in the biochemical composition, and consequently, the phenotypic profiles of T cells[1, 2, 3, 4]. For chronic infections and cancer, antigen persistence accompanied by chronic inflammation and a skewed cytokine milieu lead to alternative T cell differentiation through the "exhaustion" pathway[5]. Exhausted T cells (T_{EX}) exhibit hierarchical loss of functions, as well as unique phenotypic, transcriptional, and epigenetic profiles distinct from T_{EFF}/T_{MEM}[5, 6, 7, 8, 9, 10, 11]. However, the proteomic landscape of antigen-specific T cell differentiation *ex vivo* is understudied.

While transcriptomics captures a momentary view of RNA expression and epigenetics sheds light on gene regulation, these techniques do not directly measure the proteome, which comprises the molecular machines and functional components that drive function within a cell. Multiple studies have highlighted the limited correlation between RNA and protein levels, and the discordance between the half-lives of mRNA and their corresponding proteins[12, 13]. These include several studies aimed at proteomic profiling of immune cell activation *in vitro*, where they demonstrated the extensive remodeling of the proteome upon activation, and the heterogeneous correlation between protein abundance and mRNA quantification, thus confirming results from other fields of biology on the discordance between the proteome and transcriptome [14, 15, 16, 17, 18]. Previous studies of T cell differentiation were performed *in vitro*, often applied non-antigen specific stimulation, and were mainly focused on the early stages of T cell activation [19, 20, 21]. Other studies aimed at profiling the proteome of human immune cells in the context of viral infection or cancer; and again demonstrated that proteomic profiling highlighted proteins that were overlooked in transcriptomic data sets that have potential as immunotherapeutic targets[22, 23]. Thus, comprehensive longitudinal proteomic profiling of *ex-vivo* CD8 T cells in a well-established model is needed to dissect these aspects of molecular alterations during T cell differentiation.

Here, we profiled the dynamics of proteomic alterations during the differentiation of T cells *in vivo* in the context of acute versus chronic infection with LCMV Armstrong and Clone-13 strains, respectively. Overall, our comprehensive analysis of global protein abundance demonstrates a strong alignment with well-established knowledge of T cell biology, including key canonical markers associated with different cell states. We also identify several proteins of interest associated with T cell exhaustion and T_{EFF}/T_{MEM} differentiation previously not directly associated with T cell differentiation. Collectively, our proteomics method paired with rigorous data analyses demonstrates significant alignment with established knowledge and omics databases, confirming its overall validity and utility. Notably, we pinpoint numerous proteins potentially involved in T cell differentiation, previously overlooked, that merit further study. Due to the widespread usage and translational utility of this antigen-specific T cell stimulation model, our data promises to substantially enhance understanding of T cell differentiation and offer valuable complementary insights to other high-throughput omics approaches.

Results

Longitudinal proteomic profiling of antigen-specific CD8 T cells reveals significant modulation of the proteome upon activation followed by moderate modulations during differentiation.

Extensive characterization of T cell differentiation, encompassing phenotypic, transcriptional, and epigenetic analyses, has greatly advanced through the use of the well-established lymphocytic choriomeningitis virus (LCMV) mouse model. By comparing mice infected with the Clone 13 strain (LCMV-Cl13) causing chronic infection versus mice infected with the Armstrong strain (LCMV-Arm) causing acute infection, previous work has gained valuable insights into the molecular mechanisms of T cell differentiation and T cell exhaustion [1, 7, 10, 24, 25, 26, 27]. In this study, we employed liquid chromatography-tandem mass spectrometry (LC-MS/MS) to profile the proteome of antigen-specific T cells longitudinally at different stages of acute and chronic infections (Fig. 1A). To achieve this, we adoptively transferred transgenic CD8 T cells (P14 cells) expressing a T cell receptor (TCR) specific for the LCMV glycoprotein epitope 33-41, GP33, into two groups of congenically distinct recipient mice. One group of mice was infected with the chronic LCMV-Cl13 strain, while the other was infected with the acute LCMV-Arm strain, respectively generating exhausted T cells (T_{EX}) and effector/memory T cells (T_{EFF}/T_{MEM}). Four biological replicates were infected and analyzed independently. In each biological replicate group, P14 cells were isolated and sorted across a time course at 8, 15, and 30 days post-infection (hereafter d8, d15, and d30), representing the early, intermediate, and late stages of infection [1, 7, 10, 24, 26]. Additionally, naive P14 cells were sorted to provide a benchmark for protein expression in naive T cells (Fig. 1A, Fig. S1).

Our flow cytometry analyses reproduce previously described phenotypes of T_{EX} and T_{EFF}/T_{MEM} at the various phases of infection. This includes significantly higher expression (as measured by mean fluorescence intensity, MFI) of the canonical exhaustion markers PD-1, Tox, and CD39 (encoded by *Entpd1*) in CD8 T cells harvested from chronically Cl13-infected mice. Conversely, T_{EFF} exhibited higher levels of activation markers KLRG1, CX3CR1 (d8), and CD44 (d30), (Fig. 1B-D, Fig. S1, Fig. S2F). Furthermore, differentiation into T_{MEM} was accompanied by upregulation of the alpha subunit of interleukin-7 (IL-7) receptor, IL7Rα (CD127) (Fig. S1B). As previously reported [6, 8, 10, 24, 26], we observed that the majority of T_{EFF} (LCMV-Arm d8) exhibited the activated phenotype KLRG1^{+}PD1^{-}CD127^{-}, which shifted to the a more CD127^{+} phenotype as the cells transitioned to the T_{MEM} phenotype (LCMV-Arm d15 and d30) (Fig. 1B-D, S1, S2F). In parallel, the majority of early-T_{EX} (LCMV-Cl13 d8) displayed the PD1^{+}CD127^{-} with a significantly lower frequency of cells that are KLRG1^{+}. The frequency of KLRG1^{+} cells progressively decreased during the intermediate and late exhaustion phases (d15 and d30 LCMV-Cl13), whereas the majority of antigen-specific CD8 T cells remained PD1^{+}CD127^{-}.

Antigen-specific P14 cells from each condition (Arm and Cl13 infected mice: d8, d15, d30; and naive P14 mice) were sorted to ≥98.7% purity (Fig. S1) and processed for global protein abundance analysis. We effectively quantified over 6,600 proteins across the entire dataset and demonstrated a robust correlation in protein expression levels across all four biological replicates (Fig. S2A-B). Overall, this validates the robustness and reproducibility of our proteomics data. More importantly, the intensity of individual proteins displayed a broad dynamic range spanning

130 several orders of magnitude, encompassing transcription factors and established T cell
131 exhaustion markers such as PD-1, Lag3, and Tox (Fig. S2C-E).

132 We next confirmed concordance between the expression levels of canonical T cell
133 differentiation markers measured by flow cytometry (MFI) versus mass spectrometry-based
134 proteomics (Fig. 1D, S2F-G). Comparing markers associated with activation and effector
135 phenotype (granzyme B, CD44, CX3CR1, and KLRG1) as well as exhaustion-associated markers
136 (PD1, Tox, and Entpd1), we observe correlation between MFI and proteomics abundance for
137 every marker analyzed (Fig. S2F-G).

138 Overall, the differentiation of CD8 T cells during acute or chronic infection led to significant
139 alterations in their proteomic profile, delineated by two distinct trajectories evident in the principal
140 component analysis (PCA) (Fig. 1E). This confirmed the unique differentiation path for T_{EX} as
141 compared to the T_{EFF}/T_{MEM} on the protein level that was previously shown phenotypically[25, 26],
142 transcriptionally[10, 24], and epigenetically[1, 7]. Quantitatively, activation from the naive T cell state to
143 either early-T_{EFF} or early-T_{EX} (naive vs. d8) was accompanied by changes in the abundance of
144 ~1,000 proteins (962 and 1078 alterations for acute and chronic trajectories, respectively), which
145 is significantly higher than modulations in protein abundance occurring at further stages of
146 differentiation (d8 vs. d15 or d15 vs. d30) (Fig. 1F). Significant changes continued as the antigen-
147 specific CD8 T cells transitioned from a T_{EFF}-dominated response at the early stage of infection
148 (d8) towards a T_{MEM}-dominated response at the intermediate stage of acute infection (d15) (~200
149 proteins changing), and to a much lesser extent from intermediate to late stages (only 22 proteins
150 changed abundance). Crucially, in the context of chronic infection, significant proteome
151 modulation persisted from the early-intermediate exhaustion transition to the intermediate-late
152 exhaustion transition, involving alterations in the levels of 200 and 114 proteins, respectively.

153 Overall, the number of differentially expressed proteins observed across our time course
154 analysis of acute and chronic LCMV infections aligns with previously reported transcriptional and
155 epigenetic studies[1, 7, 10, 24]. Major modulation of the T cell proteome occurs following activation and
156 transition from the naive state, with more limited modulations observed as the cell differentiates
157 during the intermediate and late stages of infection.

158

159 **Proteomic analysis of T cell activation and differentiation in the context of acute LCMV-**
160 **Arm infection.**

161 Previous work has demonstrated key phenotypic, transcriptional, and epigenetic markers
162 and pathways in the differentiation of naive T cells into effector and subsequently into memory T
163 cells[1, 2, 3, 4, 8, 10, 24, 25, 26]. Several studies of early T cell differentiation upon *in vitro* stimulation
164 demonstrated extensive remodeling of the proteome upon activation, allowing the elucidation of
165 several novel insights into the biology of T cell activation and the specific roles of various
166 transcription factors, kinases, and environmental cues in shaping the T cell proteome[14, 16, 17, 18, 19,
167 21]. However, the *in vivo* dynamic changes of the proteome during acute infection accompanied by
168 the differentiation of naive T cells into T_{EFF}/T_{MEM} have not been studied. We analyzed protein
169 expression changes of antigen-specific CD8 P14 T cells sorted on d8, d15, and d30 post-infection
170 with acute LCMV-Arm. Our analyses revealed extensive changes of the T cell proteome upon
171 activation, where the protein abundance of 962 proteins was significantly changed as the cells
172 differentiated from naive to T_{EFF}, compared to fewer changes as the CD8 T cells transitioned from

173 the effector to the memory state as only 204 proteins significantly changed their abundance
174 between d8 and d15 post-infection with acute LCMV-Arm (Fig. 1F, S3). Very limited change was
175 observed between the intermediate (d15) and late (d30) time points, which agrees with published
176 chromatin-accessibility profiles of these cell states suggesting that the majority of changes occur
177 during activation from naive to effector cells, then many of these changes are maintained as the
178 cells differentiate to memory T cells.

179 Unsupervised clustering of longitudinal protein abundance throughout acute LCMV Arm
180 infection highlights modules of proteome alterations in the T cell proteome (Fig. 2A-B). Clusters
181 1 and 2 display consistent protein downregulation throughout the entire time course, while cluster
182 4 has delayed protein downregulation only observed from d15 onwards. Other modules exhibited
183 temporary protein downregulation. Cluster 3 showed a decrease of protein abundance at the early
184 stage of infection (d8) but regained a level of expression comparable to naive T cells by d15.
185 Similarly, protein in cluster 5 decreases at the early stage of infection (d8), then from d15 onwards
186 increases to similar or slightly higher levels than naive T cells (Fig. 2A-B).

187 The remaining clusters generally showed an increase in their relative abundance
188 compared to naive T cells with variable kinetics. Whereas clusters 6 and 7 showed a higher
189 abundance of its proteins at the early stage of infection (d8) but regained a level of expression
190 comparable to naive T cells or slightly higher by d15, clusters 8, 9, and 10 showed persistently
191 higher abundance throughout the time course compared to naive. Some biological processes
192 associated with representative clusters are represented in Fig. 2C. Proteins in cluster 6 that
193 exclusively show a higher abundance at the early stage of infection (d8) were associated with
194 DNA replication, metabolic processes, and mitotic cell processes, representing functions
195 supporting T cell replication/expansion. On the other hand, proteins in clusters 9 and 10, that
196 showed higher abundance sustained until d30, were associated with inflammatory responses,
197 leukocyte activation, and cell migration, as well as killing of cells and granzyme-mediated
198 pathways (Fig. 2C).

199 Comparing the T_{EFF} proteome from the peak of the immune response (d8) to either the
200 naive state or the d15 proteome accompanied by the T_{EFF}-to-T_{MEM} transition showed an increased
201 abundance of Ki67 (encoded by the *Mki67* gene), granzyme B (*GzmB*), and CX3CR1, whereas
202 the abundance of TCF-1 (*Tcf7*) was significantly higher in naive/T_{MEM}. For the T_{EFF}/naive
203 comparison, many other proteins were significantly more abundant in the activated and highly
204 functional T_{EFF}, such as the functional proteins GzmA, gamma-interferon (IFNγ), and perforin, the
205 activation marker CD44, as well as the transcription factors T-bet (*Tbx21*) and Zeb2.

206 Together, our longitudinal proteomic profiling of the protein abundance landscape of
207 antigen-specific CD8 T cells during acute viral infection corroborates transcriptional and
208 epigenetic trends, where extensive modulation occurs at the early stages of infection as the cell
209 exits the naive quiescent state into the activated antigen-experienced state, followed by moderate
210 changes as they differentiate from the effector to the memory state. Our results also confirmed
211 previous findings from proteomic profiling of eukaryotic cells that showed subtle differences in
212 protein abundance of specific proteins as compared to the quantification of their corresponding
213 mRNAs measured by transcriptional profiling. Importantly, several proteins previously
214 unassociated with T cell differentiation or potentially overlooked in previous transcriptomic
215 analyses, are now under investigation for their prospective roles in this context.

216

Comparison of T cell proteome changes during acute LCMV-Arm infection versus chronic LCMV-Cl13 infection.

T cell exhaustion is a hallmark of cancer and chronic viral infection and holds profound significance in the treatment of these diseases. The generation of exhausted CD8 T cells (T_{EX}) is associated with failure to clear tumor cells and virus-infected cells due to progressive hierarchical loss of functions[5, 26, 27]. T cell exhaustion represents an independent differentiation path adopted by T_{EX} distinct from the differentiation path of effector/memory T cells (T_{EFF}/T_{MEM}) generated during acute infection[1, 9, 10, 26, 28, 29, 30]. This is reflected by the unique phenotypic, metabolic, transcriptional, and epigenetic profiles distinct from T_{EFF}/T_{MEM} that start very early post-infection[24, 31, 32,33, 34, 35, 36]. In the past, the LCMV mouse model has been extensively utilized to establish foundational knowledge regarding phenotypic, metabolic, transcriptional, and epigenetic profiles of T_{EX} [24, 31, 32,33, 34, 35, 36]. We harnessed the full potential of the LCMV mouse model, which enables the comparison of antigen-specific CD8 T cells with the same specificity during both acute and chronic infection to dissect the proteome dynamics accompanying differentiation of T_{EFF}/T_{MEM} and exhausted (T_{EX}) cells.

We applied unsupervised hierarchical clustering to categorize proteome alterations of T_{EFF}/T_{MEM} T cells (from Arm infected mice) and T_{EX} T cells (from Cl13 infected mice) into distinct clusters based on their longitudinal changes (Fig. 3A-B), and performed gene ontology (GO) enrichment analysis to categorize the proteomic modules in each cluster (Fig. S4A-B). Several modules within our unsupervised clustering had elevated protein expression in T_{EX} compared to T_{EFF}/T_{MEM} (Fig. 3B). Among these, clusters 7 and 10 are associated with interferon response, cytokine production, and general adaptive immune response, and clusters 12-14 were linked to lymphocyte activation, adaptive immune response, DNA replication, and mitotic / cell cycle processes (Fig. 3B and S4B). We also observe general downregulation of respiratory chain complex 1 (Fig 3C), a known phenotype of T_{EX}, underscoring the utility of global proteomics analysis to profile cellular function.

A key benefit of analyzing infection with LCMV-Arm and LCMV-Cl13 in parallel is the ability to determine the core program of T cell differentiation versus acute-specific and chronic-specific programs. Proteins associated with the core T cell differentiation program are reflected by the intersection between Arm and Cl13 Venn diagrams, as well as proteins correlating in behavior along the diagonal axis in Fig. 3D-F. Proteins relatively higher in exhausted cells (e.g. Tigit and Lag3) or relatively lower in exhausted cells (e.g. Klrg1) deviate from the diagonal axis (Fig. 3D-F). We quantify 245, 351, and 292 differentially expressed proteins between acute and chronic infection at the early, intermediate, and late stages of infection, respectively (Fig. 1F, curved arrows). Volcano plots highlight differences in expression between T_{EX} compared to T_{EFF}/T_{MEM} at the various stages of infection, see Fig.3G (d30) and S4C-D (d8 and d15). Comparison of LCMV-Cl13 and LCMV-Arm at d30 (Fig.3G) demonstrates a significantly elevated abundance of canonical exhaustion markers for late-T_{EX} that have been extensively studied (red dots in the volcano plots). These included the inhibitory receptors (IRs) CD39 (encoded by *Entpd1*), PD1 (*Pdcd1*), TIM3 (*Havcr2*), 2B4 (*Cd244*), Lag3, and TIGIT, in addition to the transcription factors (TFs), Tox and Eomes. Additionally, proteins belonging to the interferon-stimulated genes (ISGs) Isg15, Ifit1, and Isg20, several members of the granzyme family granzyme-B, -K, and -A, the apoptosis-associated protein Caspase-3, and the proliferation marker Ki67 (*Mki67*), were significantly more abundant in T_{EX}, as previously reported. Some of these markers showed consistent higher protein abundance in T_{EX} versus T_{EFF}/T_{MEM} at the various stages of chronic

infection, including the hallmark marker of exhaustion PD1 (Pdcd1), and other checkpoints such as Lag3 and TIGIT, as well as Tox, the main TF orchestrating the exhaustion program[33, 34, 35] (Fig. S4C-D). Conversely, the activation marker KLRG1 consistently exhibited a lower abundance in T_{EX} versus T_{EFF}/T_{MEM}, in addition to a lower abundance of the memory-associated marker CD127 (*Il7r*) and TF TCF1 (*Tcf7*) at the intermediate and late stages, consistent with published signatures of T_{EX} and dysfunctional CD8 T cells (Fig. 3H). Additionally, several proteins that have not been extensively studied for their role in the T_{EX} biology showed significantly different abundance in T_{EX} versus T_{EFF}/T_{MEM}, and we are actively investigating these proteins for functional impact on T cell biology in the context of LCMV Cl13 infection.

Together, these analyses validate the application of global proteomics to identify T_{EX}-associated markers consistent with previously reported studies in the LCMV mouse model, as well as in other T cell exhaustion models and datasets. More importantly, our protein abundance profiling of T_{EX} revealed novel proteins with potential roles in exhaustion biology that require further investigation to validate their specific functions.

Integration of proteomic and transcriptomic profiling data of T cell differentiation.

Transcriptomic analysis has been pivotal to our understanding of T cell differentiation and immune cell function in general. However, previous studies have underscored the limited correlation between mRNA and protein profiling upon T cell activation *in vitro*, highlighting the significance of post-transcriptional mechanisms governing protein synthesis and degradation[20, 37, 38]. Thus, we evaluated the correlation between protein abundance and transcript quantification between T_{EX} and T_{EFF}/T_{MEM} at the different stages of infection using microarray data from Doering et al.[24] (Fig. 4A). Our analyses revealed a correlation coefficient of 0.47-0.49 for the late and intermediate time points, and even a lower correlation (0.28) for the early stage of infection, suggesting moderate to low correlation between measurements of the transcriptional changes and protein abundance changes across the different time points. These findings align with similar comparisons of protein versus transcript quantification made in diverse cellular contexts. Considering the role of protein machinery in underpinning cellular function, it is crucial to study proteomic alterations underpinning crucial cellular states such as T cell differentiation/exhaustion in primary systems, as these studies provide crucial insights into understanding the underlying molecular machinery driving cellular phenotypes and associated disease states (Fig. 4B). Since transcriptional profiling may not accurately reflect protein abundance, this discrepancy could lead to the oversight of potential biomarkers or therapeutic targets for T cell exhaustion, an issue resolved by our global proteomic analysis.

Proteomic-transcriptional correlations in a tumor mouse model demonstrates the commonality of T_{EX} biology across chronic disease.

To further validate our proteomic analysis, we compared our LCMV proteomics results with a single-cell transcriptomic data set of mouse TILs in a colon cancer model, representing an orthogonal biological context of T cell exhaustion[39]. Our analysis was based upon the observation that transcriptional expression of exhaustion-specific proteins correlates with each other across this ssRNAseq dataset (see example in Fig. S5: Lag3 vs. PD1), and that many of our T_{EX}-specific proteins also correlate with Lag3 and PD1 in transcript expression across this ssRNAseq dataset.

For our T_{EX}-specific proteins, we compared their Cl13/Arm d30 protein abundance score versus how well their single cell expression correlates PD-1 and Lag3 across the colon cancer TIL dataset [40]. This analysis revealed a positive correlation between T_{EX}-specific protein elevation and single cell RNA correlation with PD-1 and Lag3 expression (Fig. 5). Established hallmarks of exhaustion observed in our proteomics data correlated with PD-1 and Lag3 expression in the ssRNAseq dataset, as well as other novel T_{EX} proteins observed in our dataset.

Discussion

We performed the first *in vivo* longitudinal proteomic profiling of antigen-specific CD8 T cells in the context of both acute and chronic viral infection, comparing them to naive T cells. Our analyses unveil dynamic protein changes accompanying transitions between cell states in acute and chronic infections, consistent with previously reported transcriptional and epigenetic studies[1, 7, 10, 24]. The majority of proteomic modulations in T cells occur during the early stages of infection following activation, as the cells exit the naive state. Subsequent modulations during intermediate and late infection stages were more limited, particularly in the case of acute infection. Our longitudinal proteomic profiling during acute viral infection corroborated with previously published transcriptional and epigenetic characterization of these cells, however, several proteins identified by our proteomics approach were previously not investigated for their role in T cell differentiation during acute infection, warranting further investigation to elucidate their potential roles. By concurrently analyzing acute LCMV-Arm and LCMV-Cl13, we identified common proteomic modules, suggesting a core proteomic program of T cell differentiation, as well as acute-specific and chronic-specific programs. Analysis of the LCMV-Cl13 chronic infection setting revealed T_{EX}-associated established markers that agree with previously reported transcriptional and epigenetic profiling in the same LCMV mouse model, as well as in other T cell exhaustion/dysfunction models and datasets. Importantly, our protein abundance profiling of T_{EX} revealed novel proteins with potential roles in exhaustion biology that necessitate investigation to validate their specific functions.

The fields of immunology and immunotherapy are on a quest for novel interventions to enhance the efficacy and durability of immunotherapy[41, 42]. One overlooked and understudied aspect of T cell biology is profiling the biochemical alterations within the cells, including the protein abundance changes. Despite several endeavors to characterize modulation of the protein abundance of T cells upon activation *in vitro* and the profiling of cells from human samples *ex-vivo*, the direct *ex-vivo* mapping of the proteome associated with the different states of T cell differentiation under various conditions is lacking. This data is essential since it could bring valuable insights into biochemical networks driving the T cell effector/memory and exhaustion programs, as well as identify novel roles of specific proteins in the differentiation of T cells that might have been overlooked due to discrepancies between the gene expression levels measured by transcriptional profiling and the actual protein abundance which could only be resolved by proteomic profiling. Future work will focus on dissecting the specific role of newly reported proteins in our dataset in T cell differentiation, and their impact in the modulation of the protein interactome of CD8 T cells. Delving into the potential roles of these lesser-known proteins in T_{EX} biology could uncover promising targets for drug development.

Author contributions

MSA and DEG conceived the experiments. ASD and AO performed CMV infections and flow cytometry experiments with help from AF, SM, CN, AA, and CR. SM and CN provided technical help with flow cytometry panels. ASD was responsible for mouse breeding and colony maintenance with help from AAG. CMB and SLW performed the proteomics analysis with support from CMM. CMB performed bioinformatic analyses and prepared figures. MSA, CMB, and DEG prepared the manuscript.

Acknowledgments

This work was supported by Emory MP3 Seed Grant (00121861), and the Department of Pathology and Laboratory Medicine Start-up funds to MSA and DEG. CMB was supported by a Swedish Research Council grant (2023-00510). ASF is supported by an NIH IMSD T32 Graduate Fellowship. The authors would like to thank members of Hakeem and Gordon labs, as well as members of PATRU and EVC for their valuable discussions and comments. We would also like to thank the Emory Flow Cytometry Core and the Emory Integrated Genomics Core for their support.

365 **Materials & Methods**

366

367 **Mice**

368 Age and sex-matched C57BL/6 mice (CD45.2+) from The Jackson Laboratory between the ages
369 of 5-7 weeks, were used for all infection experiments. Both male and female mice were used in
370 the study. P14 TCR transgenic mice expressing a TCR specific for the H-2D^b GP33-41 epitope of
371 LCMV were bred at Emory University. Transgenic P14 CD8 T cells were harvested from mice
372 aged between 6-24 weeks from donor P14 mice matching the gender of the recipient mice. Mice
373 were maintained in a temperature-controlled animal facility at Emory University with a 12-h
374 light/dark cycle. All experimental procedures and breeding conditions were in accordance with
375 Institutional Animal Care and Use Committee (IACUC) guidelines for Emory University.

376

377 **Adoptive T cell transfer and LCMV infections**

378 Peripheral blood mononuclear cells (PBMCs) containing P14 CD8+ T cells (CD45.1$^+$) were
379 adoptively transferred intravenously (i.v.) into recipient mice (CD45.2$^+$) one day before infection
380 with LCMV. Recipient mice were engrafted with either 5×10^3 P14 cells for LCMV-Arm, and 1×10^3
381 P14 cells for LCMV-Cl13. For acute viral infections, mice were injected intraperitoneally (i.p) with
382 2×10^5 plaque-forming units (PFU) of LCMV-Arm. For chronic viral infections, mice were injected
383 i.v. with 4×10^6 PFU of LCMV-Cl13. LCMV-Arm and Cl13 were grown in BHK cells (ATCC, catalog
384 no. CCL-10) at a multiplicity of 0.01, 0.02 and/or 0.1 and supernatants were harvested at 60h
385 post-infection. Viral productions were titrated on VERO cells (ATCC, catalog no. CCL-81) using
386 plaque assay as previously described[43].

387

388 **Cell preparation**

389 Spleens isolated from mice at each time point (days 8, 15, and 30) post-infections with LCMV-
390 Arm and Cl13, were collected and homogenized together as a pooled sample using 70-µm cell
391 strainers. Cells were then centrifuged at 500x *g* for 5 minutes at 4ºC. After removing the
392 supernatant, the cell pellet was resuspended in ammonium-chloride-potassium (ACK) lysis buffer
393 and incubated for 3 minutes at room temperature to lyse the red blood cells. After incubation, an
394 additional 20 mL of RPMI + 1% fetal bovine serum (FBS) was added to neutralize the lysis buffer,
395 and the cells were centrifuged at 500x *g* for 5 minutes at 4ºC. The resulting cell pellet was
396 resuspended in RPMI + 10% FBS, and then counted. The splenocytes were then used for flow
397 cytometry and cell sorting. Before cell sorting, CD8+ T cells were enriched from total splenocytes
398 using the EasySep™ Mouse CD8+ T Cell Isolation Kit (STEMCELL Technologies) (routinely
399 >90% purity).

400

401 **Antibodies, flow cytometry and cell sorting**

402 The following fluorochrome-conjugated antibodies were used (clone mentioned in parentheses).
403 From Biolegend: anti-CD44–BV785 (IM7), dilution 1:300; anti-CD45.1–A700 (A20), 1:200; anti-
404 CD69–BV785 (H1.2F3), 1:200; anti-CD127–PE-Cy5 (A7R34), 1:200; anti-PD-1–PE-Cy7 (RMP1-
405 30), 1:200; anti-PD-1–APC-Fire 810 (29F.1A12), 1:200; anti-TIM3–BV605 (RMT3-23), 1:200;

anti-CX3CR1–BV650 (SA011F11), 1:200. From BD Biosciences: anti-CD8–BV650 (53–6.7), 1:200; anti-CD8–BUV805 (53–6.7), 1:200; anti-CD44–BUV737 (IM7), 1:200; anti-CD45.1–FITC (A20), 1:200; anti-CD45.1–BUV496 (A20), 1:200; anti-CD39–BV711 (Y23-1185), 1:200; anti-PD-1–BV786 (29F.1A12), 1:200; anti-Ly108–BB700 (13G3), 1:200; anti-granzyme–PE-CF594 (GB12), 1:100; anti-TCF-1/TCF7–R718 (S33-966), 1:100. From ThermoFisher Scientific: anti-CD101–PE-Cy7 (Moushi101), 1:100; Live/Dead Fixable Aqua Dead Cell Stain Kit, 1:500; Live/Dead Fixable Blue Dead Cell Stain Kit, 1:500. From Miltenyi Biotec: anti-TOX–APC (REA473), 1:100. From Southern Biotech: anti-KLRG1–FITC (2F1), 1:150. Tetramers of MHC class I H-2D^b GP33 were obtained from the NIH Tetramer Facility, Emory University, dilution 1:500.

Flow cytometry surface staining was performed by incubating cells with indicated antibodies for 20 minutes at 4°C. Intracellular staining was conducted with the eBioscience™ Foxp3/Transcription Factor Fixation/Permeabilization Kit (Thermo Fisher Scientific). Flow cytometry data were obtained using BD FACSymphony™ A5 prior to sorting to examine the phenotypes of LCMV-specific CD8 T cells. Subsequently, Cytek Aurora (Cytek Biosciences) was used to achieve greater depth in phenotypic analysis. Data were analyzed using FlowJo™ v10.10 Software (FlowJo, LLC).

The enriched CD8+ T cells were stained on ice for 30 minutes with the relevant antibodies cocktail. P14 cells (CD45.1$^+$GP33$^+$) were sorted with a FACS Aria II (BD Biosciences) using a 100-µM nozzle in RPMI supplemented with 10% FBS filtered with 0.22 µM filter. P14 cells were sorted from different time points on days 8, 15, and 30 post-infections with LCMV in four replicate experiments. Naive P14 cells were also sorted to provide a benchmark for protein expression in naive T cells. At least 2x10^5 antigen-specific CD8 T cells were sorted from the different samples. Following FACS sorting, cells were washed twice in ice-cold PBS and frozen pellets were used for proteomics analysis. Sorted cells were washed twice in PBS and snap-frozen at -80 °C.

Proteomics sample preparation

Cell pellets were resuspended in 100 mM Tris pH 8, supplemented with 0.1% DDM, 10 mM TCEP, and 40 mM CAA. Samples were boiled for 10 min at 95 °C and sonicated in a Bioruptor (Diagenode) for 10 cycles of 30 sec on/30 sec off. The protein amount was determined by BCA following manufacturer instructions (Thermo Fisher Scientific) and samples were digested overnight with a 1:100 (w/w) Trypsin/Lys-C Mix (Promega) at 37 °C. 200 ng of peptides were loaded onto preconditioned EvoTips (EvoSep) and washed following manufacturer instructions.

LC-MS/MS

Samples were injected in an EvoSep One system (EvoSep) coupled to a timsTOF Pro2 mass-spectrometer (Bruker Daltonics). The peptides were loaded on a 15 cm Aurora Elite CSI column (IonOpticks) and chromatographic separation was achieved using the predefined 20 SPD method. The mass-spectrometer operated in positive polarity for data collection using data-independent acquisition (diaPASEF) mode[44]. DIA isolation windows were optimized by py_diAID, consisting of 4 ion mobility windows and 12 mass isolation windows[45]. All spectra were acquired within an m/z range of 100 to 1700 and fragmentation energy was set to 20 eV at 0.85 1/K0 and 59 eV at 1.30 1/K0.

449

450 **Proteomics data analysis**

451 Protein identification and quantification were performed using Spectronaut[46] (version 18) in
452 library-free mode using the Mus musculus SwissProt database (UP000000589; downloaded on
453 7.1.2022; 17,090 entries) with default settings. Modifications were defined as follows,
454 Carbamidomethylation (C) as a fixed modification, and Acetyl (Protein N-term) and Oxidation (M)
455 as variable modifications. All further data processing was performed in R (version 4.3.1). Only
456 proteins with at least 3 quantified values in at least one sample group were kept. Intensities were
457 normalized by median centering and log_2-scaling. Missing values were imputed by Bayesian PCA
458 imputation[47] and downshift sampling, for proteins missing at random or not at random,
459 respectively[48]. All statistical comparisons between the two groups were performed based on two-
460 tailed Student's t-tests. For analysis across multiple groups, ANOVA was employed. Gene
461 ontology enrichment analysis was performed in Metascape, defining all identified proteins as
462 background[49]. CellMarker analysis was performed with Enrichr, using the default setting[50].
463 Correlations are reported as Pearson correlation unless otherwise noted. A p-value below 0.05
464 was considered statistically significant.

465

466 **Integration of RNA sequencing data set**

467 Public Microarray data from *Doering et al.* was downloaded from the original publication and the
468 Gene Omnibus website[24]. Single-cell transcriptomics (scRNASeq) data from mouse TILs were
469 downloaded from *Andreatta et al*[39]. Correlation of scRNAseq data was performed with CS-CORE,
470 using default settings[40]. To increase the robustness of the correlation approach, only gene
471 products with an average read count of at least 0.2 in one of the cellular subsets, as defined in
472 the original publication, were considered.

473 **Data availability**

474 The mass spectrometry proteomics data files will be deposited to the ProteomeXchange
475 Consortium via the PRIDE partner repository[51].

476

477

478 **Figure legends**

479

480 **Figure 1: Longitudinal proteomic profiling of antigen-specific CD8 T highlighting the**
481 **differential expression of proteins in acute versus chronic conditions.** (**A**) Experimental
482 strategy detailing the profiling proteome-wide alteration in CD8+ T cell differentiating in acute
483 resolving and chronic viral infections. (**B, C**) Representative flow cytometry dot plots
484 demonstrating the levels of the canonical exhaustion marker PD-1 and the antigen-experienced
485 marker Klrg1. (**D**) Comparison of protein expression assessed through flow cytometry (top) and
486 mass spectrometry-based proteomics (bottom). The absence of a measurement bar indicates no
487 quantification. (**E**) Principal component analysis (PCA) across all proteomics samples. (**F**)
488 Quantification of protein abundance alterations across the T cell differential axis in acute resolving
489 and chronic viral infections. Dark wedges represent up-regulated proteins ($p < 0.05$ from one-
490 sided ANOVA, absolute $\log_2FC > 1$), while grey wedges signify down-regulated proteins ($p < 0.05$
491 from one-sided ANOVA, absolute $\log_2FC > 1$). Curved lines represent the number of differentially
492 expressed proteins comparing Cl13 vs Arm at each time point post-infection (higher in arrowhead-
493 facing sample). N = 4 for all proteomics samples, with error bars representing mean ± standard
494 deviation. Naive B6 mice were used as staining controls in (D).

495

496 **Figure 2: Expression profiles of proteins defining T cell activation and differentiation in the**
497 **context of acute LCMV-Arm infection.** (**A**) Unsupervised hierarchical clustering of differentially
498 expressed proteins ($p < 0.05$ from one-sided ANOVA and absolute log2FC > 1) accompanying
499 LCMV Arm (acute) infection time course. (**B**) Longitudinal protein changes for proteins within
500 selected clusters. The bold line represents the average protein change from each cluster. (**C**)
501 Gene ontology enrichment analysis of selected protein clusters. (**D, E, F**) Protein alterations were
502 observed along the differentiation transition from naive to effector/memory antigen-specific T
503 cells. P-values were calculated using a two-sided Student t-test with equal variance.

504

505 **Figure 3: Common and distinct dynamic changes of the T cell proteome in the context of**
506 **acute LCMV-Arm and chronic LCMV-Cl13 infections.** (**A**) Unsupervised hierarchical clustering
507 of differentially expressed proteins across post-infection conditions ($p < 0.05$ from one-sided
508 ANOVA and absolute log2FC > 1). (**B**) Comparison of protein alterations between acute and
509 chronic T cells for each cluster. (**C**) Distribution of protein expression changes belonging to the
510 respiratory chain complex 1 across all samples. (**D**, **E**, **F**) Scatter plots comparing protein
511 expression changes of acute and chronic infected T cells versus Naive on days 8, 15, and 30. (**G**)
512 Volcano plot of differential protein abundance in CD8 T cells isolated from mice infected with
513 Armstrong versus Clone 13 strains 30 days post-infection. (**H**) Protein signatures of statically
514 regulated proteins from (G), extracted by CellMarker[50]. N = 4 for all proteomics samples. Sample
515 correlation was determined using Pearson correlation. The Jaccard index was employed to
516 compare statically significant regulated proteins ($p < 0.05$, absolute $\log_2FC > 1$).

517

518 **Figure 4: Comparison of T cell transcriptional and proteomics analysis reveals limited**
519 **correlation.** (**A**) Scatter plots comparing proteomics data with microarray data from *Doering et*
520 *al*. for each time point post-infection. (**B**) Evaluation of microarray depth concerning significantly

521 regulated proteins identified by either microarray data from Doering *et al*.[24] or proteomics
522 experiments. Sample correlation was determined using Pearson correlation.

523

524 **Figure 5: Validation of the proteomic-transcriptional correlation in an orthogonal tumor**
525 **mouse model. (A)** Correlation analysis of single-cell RNA transcriptomics measurements
526 conducted by CS-Core[40]. (**B, C**) Scatter plots illustrating the correlation of genes with PD-1 and
527 Lag3 expression, comparing results from *Andretta et al.*[39], with proteomics measurements.
528 Scatter plot correlation (R) was computed using Spearman correlation.

529 **Supplementary Figure legends**

530

531 **Supplementary Figure S1: Flow cytometry validation of the phenotype and sorting purity**
532 **of antigen-specific CD8 T cells used for proteomic profiling by MassSpec.** (**A**)
533 Representative dot plots reflecting the sorting purity (post-sorting, right panels) compared to the
534 original frequencies pre-sorting. (**B**) Gating strategy for flow cytometry analysis. (**C**)
535 Representative dot plots of the phenotypic analysis of antigen-specific CD8 T cells.

536

537 **Supplementary Figure S2: Logistics of protein abundance profiling of antigen-specific CD8**
538 **T cells in the context of acute and chronic infection.** (**A**) Number of quantified proteins in each
539 proteomics sample. (**B**) Correlation between the different samples from all four biological
540 replicates. (**C-E**) Dynamic range for the protein abundance quantification for the naive (**C**), acute
541 (**D**), and chronic (**E**) samples. (**F**) Comparison of protein expression assessed through flow
542 cytometry (top) and proteomics (bottom). The absence of a measurement bar indicates no
543 quantification. (**G**) Correlation (Pearson) between protein expression levels assessed through
544 flow cytometry (Y-axis) and proteomics (X-axis). Naive B6 mice were used as staining controls
545 in (F-G).

546

547

548 **Supplementary Figure S3: Protein abundance alterations associated with T cell**
549 **differentiation during acute viral infection.** (**A**) Quantification of protein abundance
550 alterations across the T cell differential axis in acute LCMV (Arm) infection. (**B**) Significant
551 differentially expressed protein intersections at the different time points post-infection with acute
552 LCMV-Arm compared to naive CD8 T cells ($p < 0.05$ from one-sided ANOVA, absolute $\log_2 FC >$
553 1).

554

555 **Supplementary Figure S4: Protein alterations in the context of T cell exhaustion**
556 **compared to differentiation in an acute context.** (**A**) Differentially expressed proteins were
557 identified among the highlighted conditions ($p < 0.05$ from one-sided ANOVA, absolute $\log_2 FC >$
558 1). (**B**) Biological processes associated with differentially expressed proteins clustered in Figure
559 3A and B. (**C-D**) Volcano plots depicting differential protein quantification in CD8 T cells harvested
560 following Armstrong or Clone 13 infection at 8 (**C**) or 15 (**D**) days post-infection.

561

562 **Supplementary Figure S5: Correlation of PD1 and LAG3 gene expression in a mouse tumor**
563 **model of colon cancer.** Correlation of Pdcd1 and Lag3 across scRNAseq data in a mouse colon
564 cancer model.

565 **References**

566

567 1. Scott-Browne, J.P. *et al.* Dynamic Changes in Chromatin Accessibility Occur in CD8(+) T
568 Cells Responding to Viral Infection. *Immunity* **45**, 1327-1340 (2016).

569

570 2. Kaech, S.M. *et al.* Selective expression of the interleukin 7 receptor identifies effector
571 CD8 T cells that give rise to long-lived memory cells. *Nat Immunol* **4**, 1191-1198 (2003).

572

573 3. Joshi, N.S. *et al.* Inflammation directs memory precursor and short-lived effector CD8(+)
574 T cell fates via the graded expression of T-bet transcription factor. *Immunity* **27**, 281-295
575 (2007).

576

577 4. Hudson, W.H. *et al.* Expression of novel long noncoding RNAs defines virus-specific
578 effector and memory CD8(+) T cells. *Nat Commun* **10**, 196 (2019).

579

580 5. McLane, L.M., Abdel-Hakeem, M.S. & Wherry, E.J. CD8 T Cell Exhaustion During
581 Chronic Viral Infection and Cancer. *Annu Rev Immunol* **37**, 457-495 (2019).

582

583 6. Blackburn, S.D. *et al.* Coregulation of CD8+ T cell exhaustion by multiple inhibitory
584 receptors during chronic viral infection. *Nat Immunol* **10**, 29-37 (2009).

585

586 7. Ghoneim, H.E. *et al.* De Novo Epigenetic Programs Inhibit PD-1 Blockade-Mediated T
587 Cell Rejuvenation. *Cell* **170**, 142-157 e119 (2017).

588

589 8. Kaech, S.M. & Cui, W. Transcriptional control of effector and memory CD8+ T cell
590 differentiation. *Nat Rev Immunol* **12**, 749-761 (2012).

591

592 9. Pauken, K.E. *et al.* Epigenetic stability of exhausted T cells limits durability of
593 reinvigoration by PD-1 blockade. *Science* **354**, 1160-1165 (2016).

594

595 10. Wherry, E.J. *et al.* Molecular signature of CD8+ T cell exhaustion during chronic viral
596 infection. *Immunity* **27**, 670-684 (2007).

597

598 11. Wherry, E.J. & Kurachi, M. Molecular and cellular insights into T cell exhaustion. *Nat*
599 *Rev Immunol* **15**, 486-499 (2015).

600

601 12. Wang, D. *et al.* A deep proteome and transcriptome abundance atlas of 29 healthy
602 human tissues. *Mol Syst Biol* **15**, e8503 (2019).
603
604 13. Edfors, F. *et al.* Gene-specific correlation of RNA and protein levels in human cells and
605 tissues. *Mol Syst Biol* **12**, 883 (2016).
606
607 14. Damasio, M.P. *et al.* Extracellular signal-regulated kinase (ERK) pathway control of
608 CD8+ T cell differentiation. *Biochem J* **478**, 79-98 (2021).
609
610 15. Howden, A.J.M. *et al.* Quantitative analysis of T cell proteomes and environmental
611 sensors during T cell differentiation. *Nat Immunol* **20**, 1542-1554 (2019).
612
613 16. Hukelmann, J.L. *et al.* The cytotoxic T cell proteome and its shaping by the kinase
614 mTOR. *Nat Immunol* **17**, 104-112 (2016).
615
616 17. Marchingo, J.M., Sinclair, L.V., Howden, A.J. & Cantrell, D.A. Quantitative analysis of
617 how Myc controls T cell proteomes and metabolic pathways during T cell activation. *Elife*
618 **9** (2020).
619
620 18. Ross, S.H., Rollings, C.M. & Cantrell, D.A. Quantitative Analyses Reveal How Hypoxia
621 Reconfigures the Proteome of Primary Cytotoxic T Lymphocytes. *Front Immunol* **12**,
622 712402 (2021).
623
624 19. Rieckmann, J.C. *et al.* Social network architecture of human immune cells unveiled by
625 quantitative proteomics. *Nat Immunol* **18**, 583-593 (2017).
626
627 20. Wolf, T. *et al.* Dynamics in protein translation sustaining T cell preparedness. *Nat*
628 *Immunol* **21**, 927-937 (2020).
629
630 21. Joshi, R.N. *et al.* TcellSubC: An Atlas of the Subcellular Proteome of Human T Cells.
631 *Front Immunol* **10**, 2708 (2019).
632
633 22. Canale, F.P. *et al.* Proteomics of immune cells from liver tumors reveals immunotherapy
634 targets. *Cell Genom* **3**, 100331 (2023).
635
636 23. Jiang, Y. *et al.* Proteomics identifies new therapeutic targets of early-stage
637 hepatocellular carcinoma. *Nature* **567**, 257-261 (2019).

638

639 24. Doering, T.A. *et al.* Network analysis reveals centrally connected genes and pathways
640 involved in CD8+ T cell exhaustion versus memory. *Immunity* **37**, 1130-1144 (2012).

641

642 25. Fuller, M.J. & Zajac, A.J. Ablation of CD8 and CD4 T cell responses by high viral loads.
643 *J Immunol* **170**, 477-486 (2003).

644

645 26. Wherry, E.J., Blattman, J.N., Murali-Krishna, K., van der Most, R. & Ahmed, R. Viral
646 persistence alters CD8 T-cell immunodominance and tissue distribution and results in
647 distinct stages of functional impairment. *J Virol* **77**, 4911-4927 (2003).

648

649 27. Zajac, A.J. *et al.* Viral immune evasion due to persistence of activated T cells without
650 effector function. *J Exp Med* **188**, 2205-2213 (1998).

651

652 28. Sen, D.R. *et al.* The epigenetic landscape of T cell exhaustion. *Science* **354**, 1165-1169
653 (2016).

654

655 29. Bengsch, B. *et al.* Bioenergetic Insufficiencies Due to Metabolic Alterations Regulated by
656 the Inhibitory Receptor PD-1 Are an Early Driver of CD8(+) T Cell Exhaustion. *Immunity*
657 **45**, 358-373 (2016).

658

659 30. Scott-Browne, J.P. *et al.* Dynamic Changes in Chromatin Accessibility Occur in CD8+ T
660 Cells Responding to Viral Infection. *Immunity* **45**, 1327-1340 (2016).

661

662 31. Paley, M.A. *et al.* Progenitor and terminal subsets of CD8+ T cells cooperate to contain
663 chronic viral infection. *Science* **338**, 1220-1225 (2012).

664

665 32. Shin, H. *et al.* A role for the transcriptional repressor Blimp-1 in CD8(+) T cell exhaustion
666 during chronic viral infection. *Immunity* **31**, 309-320 (2009).

667

668 33. Alfei, F. *et al.* TOX reinforces the phenotype and longevity of exhausted T cells in
669 chronic viral infection. *Nature* **571**, 265-269 (2019).

670

671 34. Khan, O. *et al.* TOX transcriptionally and epigenetically programs CD8(+) T cell
672 exhaustion. *Nature* **571**, 211-218 (2019).

673

674 35. Scott, A.C. *et al.* TOX is a critical regulator of tumour-specific T cell differentiation.
675 *Nature* **571**, 270-274 (2019).
676
677 36. Yao, C. *et al.* Single-cell RNA-seq reveals TOX as a key regulator of CD8(+) T cell
678 persistence in chronic infection. *Nat Immunol* **20**, 890-901 (2019).
679
680 37. Nicolet, B.P. & Wolkers, M.C. The relationship of mRNA with protein expression in CD8+
681 T cells associates with gene class and gene characteristics. *PLoS One* **17**, e0276294
682 (2022).
683
684 38. Tan, H. *et al.* Integrative Proteomics and Phosphoproteomics Profiling Reveals Dynamic
685 Signaling Networks and Bioenergetics Pathways Underlying T Cell Activation. *Immunity*
686 **46**, 488-503 (2017).
687
688 39. Andreatta, M. *et al.* Interpretation of T cell states from single-cell transcriptomics data
689 using reference atlases. *Nat Commun* **12**, 2965 (2021).
690
691 40. Su, C. *et al.* Cell-type-specific co-expression inference from single cell RNA-sequencing
692 data. *Nat Commun* **14**, 4846 (2023).
693
694 41. Saez-Ibanez, A.R., Upadhaya, S. & Campbell, J. Immuno-oncology clinical trials take a
695 turn beyond PD1/PDL1 inhibitors. *Nat Rev Drug Discov* **22**, 442-443 (2023).
696
697 42. Saez-Ibanez, A.R., Sommers, E., Upadhaya, S. & Campbell, J. PD1/PDL1 clinical trials
698 adapt to a growing landscape of patients resistant to PDx. *Nat Rev Drug Discov* **22**, 944-
699 945 (2023).
700
701 43. Welsh, R.M. & Seedhom, M.O. Lymphocytic choriomeningitis virus (LCMV): propagation,
702 quantitation, and storage. *Curr Protoc Microbiol* **Chapter 15**, Unit 15A 11 (2008).
703
704 44. Meier, F. *et al.* diaPASEF: parallel accumulation-serial fragmentation combined with
705 data-independent acquisition. *Nat Methods* **17**, 1229-1236 (2020).
706
707 45. Skowronek, P. *et al.* Rapid and In-Depth Coverage of the (Phospho-)Proteome With
708 Deep Libraries and Optimal Window Design for dia-PASEF. *Mol Cell Proteomics* **21**,
709 100279 (2022).
710

711 46. Bruderer, R. *et al.* Optimization of Experimental Parameters in Data-Independent Mass
712 Spectrometry Significantly Increases Depth and Reproducibility of Results. *Mol Cell*
713 *Proteomics* **16**, 2296-2309 (2017).

714

715 47. Jin, L. *et al.* A comparative study of evaluating missing value imputation methods in
716 label-free proteomics. *Sci Rep* **11**, 1760 (2021).

717

718 48. Lazar, C., Gatto, L., Ferro, M., Bruley, C. & Burger, T. Accounting for the Multiple
719 Natures of Missing Values in Label-Free Quantitative Proteomics Data Sets to Compare
720 Imputation Strategies. *J Proteome Res* **15**, 1116-1125 (2016).

721

722 49. Zhou, Y. *et al.* Metascape provides a biologist-oriented resource for the analysis of
723 systems-level datasets. *Nat Commun* **10**, 1523 (2019).

724

725 50. Hu, C. *et al.* CellMarker 2.0: an updated database of manually curated cell markers in
726 human/mouse and web tools based on scRNA-seq data. *Nucleic Acids Res* **51**, D870-
727 D876 (2023).

728

729 51. Vizcaino, J.A. *et al.* ProteomeXchange provides globally coordinated proteomics data
730 submission and dissemination. *Nat Biotechnol* **32**, 223-226 (2014).

731

732

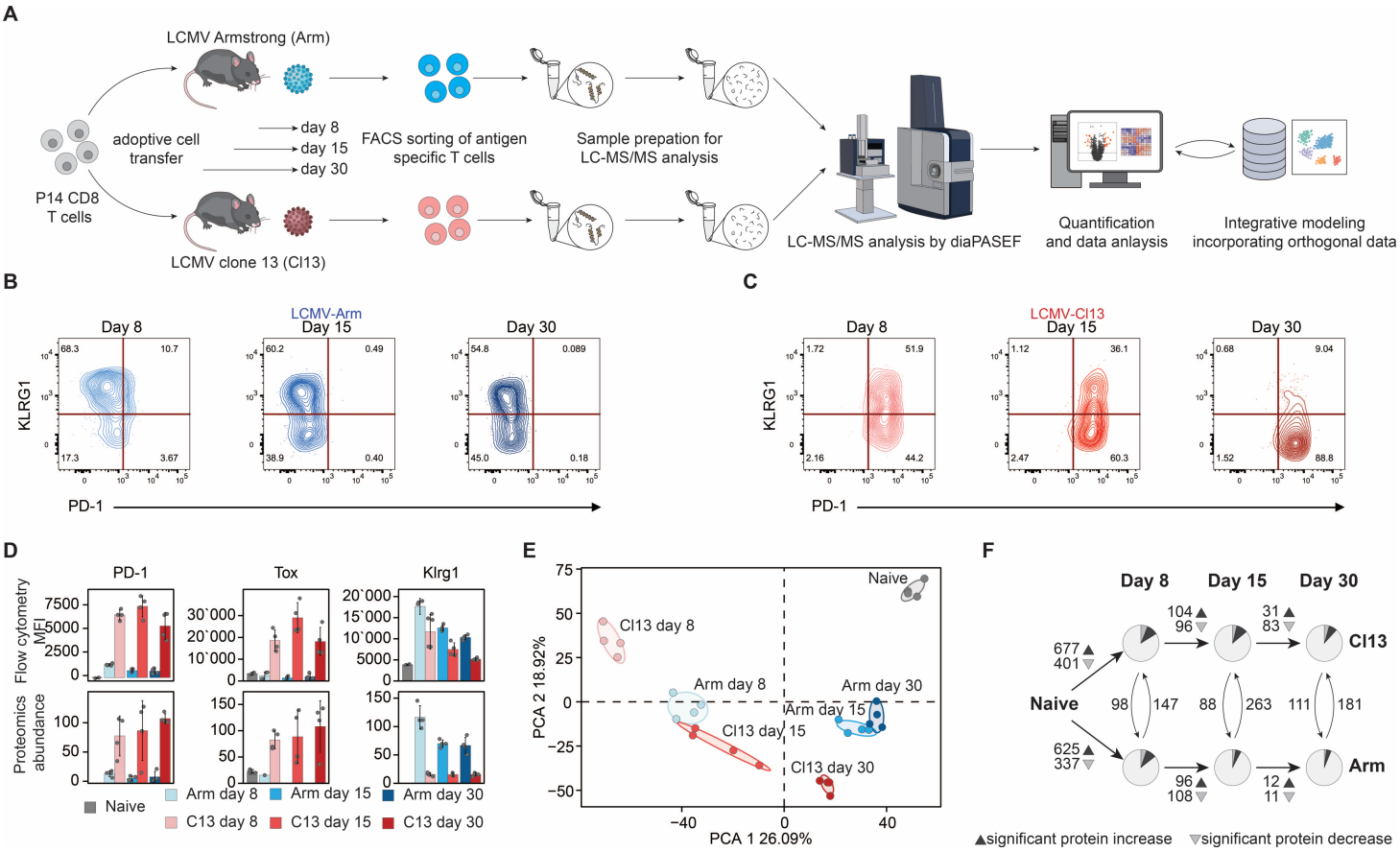

Figure 1: Longitudinal proteomic profiling of antigen-specific CD8 T highlighting the differential expression of proteins in acute versus chronic conditions. (**A**) Experimental strategy detailing the profiling proteome-wide alteration in CD8+ T cell differentiating in acute resolving and chronic viral infections. (**B, C**) Representative flow cytometry dot plots demonstrating the levels of the canonical exhaustion marker PD-1 and the antigen-experienced marker Klrg1. (**D**) Comparison of protein expression assessed through flow cytometry (top) and mass spectrometry-based proteomics (bottom). The absence of a measurement bar indicates no quantification. (**E**) Principal component analysis (PCA) across all proteomics samples. (**F**) Quantification of protein abundance alterations across the T cell differential axis in acute resolving and chronic viral infections. Dark wedges represent up-regulated proteins ($p < 0.05$ from one-sided ANOVA, absolute $\log_2FC > 1$), while grey wedges signify down-regulated proteins ($p < 0.05$ from one-sided ANOVA, absolute $\log_2FC > 1$). Curved lines represent the number of differentially expressed proteins comparing Cl13 vs Arm at each time point post-infection (higher in arrowhead-facing sample). N = 4 for all proteomics samples, with error bars representing mean ± standard deviation. Naive B6 mice were used as staining controls in (D).

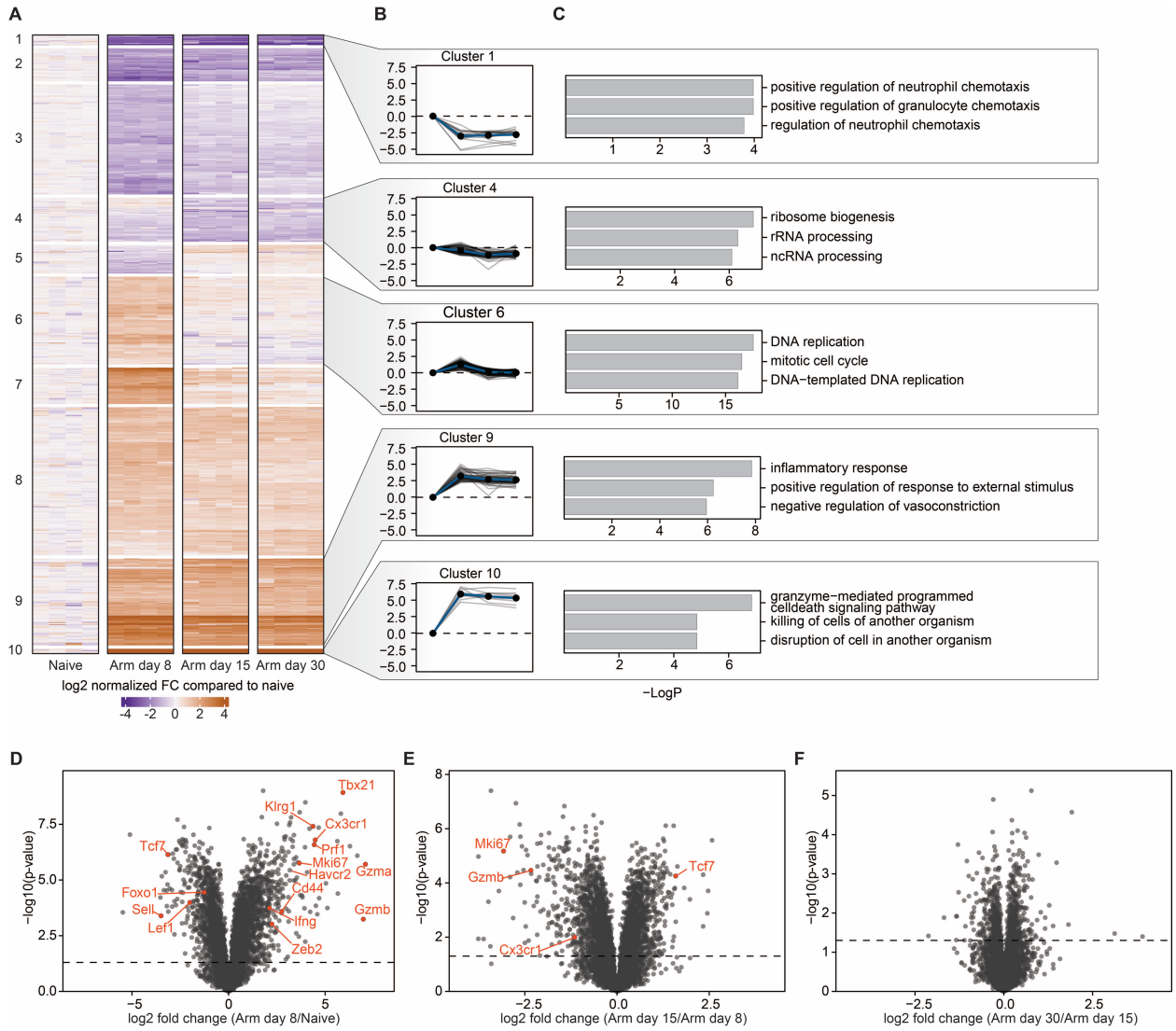

Figure 2: Expression profiles of proteins defining T cell activation and differentiation in the context of acute LCMV-Arm infection. (**A**) Unsupervised hierarchical clustering of differentially expressed proteins ($p < 0.05$ from one-sided ANOVA and absolute log2FC > 1) accompanying LCMV Arm (acute) infection time course. (**B**) Longitudinal protein changes for proteins within selected clusters. The bold line represents the average protein change from each cluster. (**C**) Gene ontology enrichment analysis of selected protein clusters. (**D, E, F**) Protein alterations were observed along the differentiation transition from naive to effector/memory antigen-specific T cells. P-values were calculated using a two-sided Student t-test with equal variance.

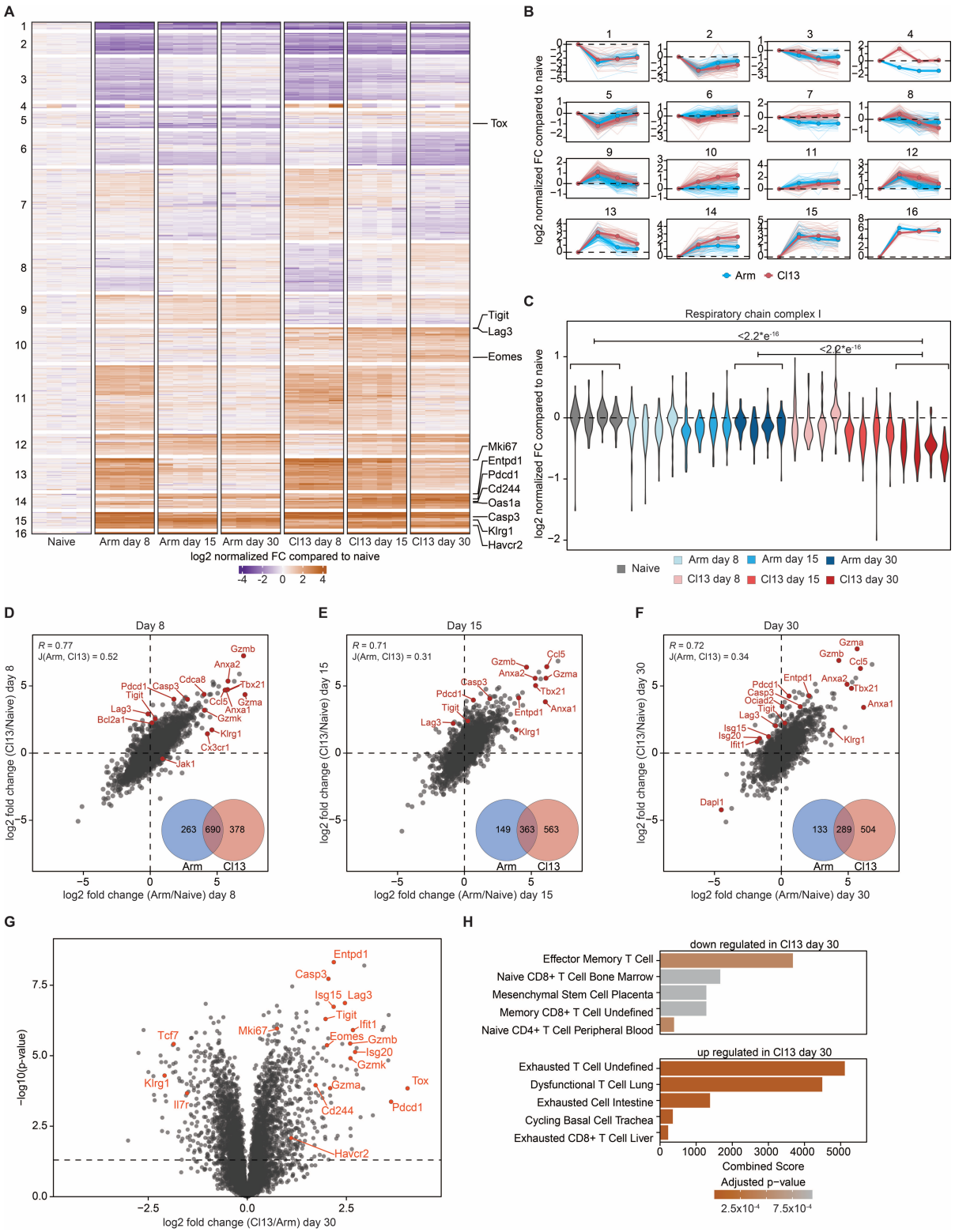

Figure 3: Common and distinct dynamic changes of the T cell proteome in the context of acute LCMV-Arm and chronic LCMV-Cl13 infections. (**A**) Unsupervised hierarchical clustering of differentially expressed proteins across post-infection conditions ($p < 0.05$ from one-sided ANOVA and absolute log2FC > 1). (**B**) Comparison of protein alterations between acute and chronic T cells for each cluster. (**C**) Distribution of protein expression changes belonging to the respiratory chain complex 1 across all samples. (**D**, **E**, **F**) Scatter plots comparing protein expression changes of acute and chronic infected T cells versus Naive on days 8, 15, and 30. (**G**) Volcano plot of differential protein abundance in CD8 T cells isolated from mice infected with Armstrong versus Clone 13 strains 30 days post-infection. (**H**) Protein signatures of statically regulated proteins from (G), extracted by CellMarker[50]. N = 4 for all proteomics samples. Sample correlation was determined using Pearson correlation. The Jaccard index was employed to compare statically significant regulated proteins ($p < 0.05$, absolute $log_2FC > 1$).

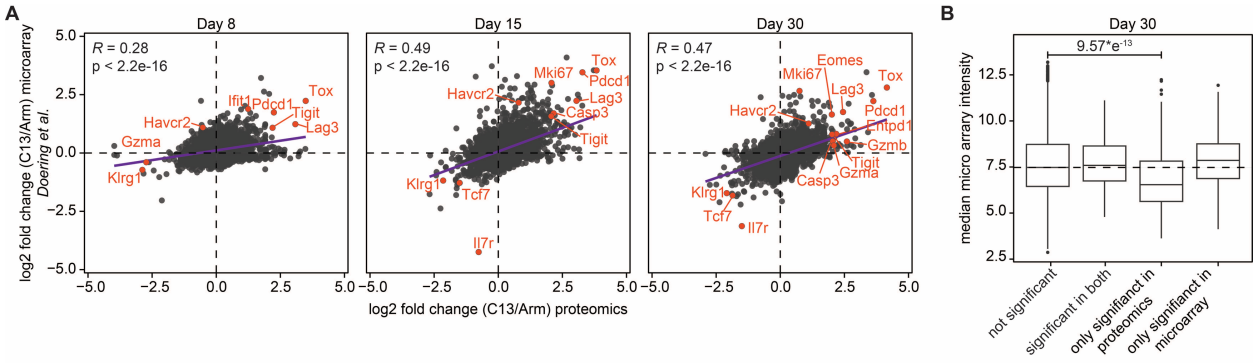

Figure 4: Comparison of T cell transcriptional and proteomics analysis reveals limited correlation. (**A**) Scatter plots comparing proteomics data with microarray data from *Doering et al*. for each time point post-infection. (**B**) Evaluation of microarray depth concerning significantly regulated proteins identified by either microarray data from Doering *et al*.[24] or proteomics experiments. Sample correlation was determined using Pearson correlation.

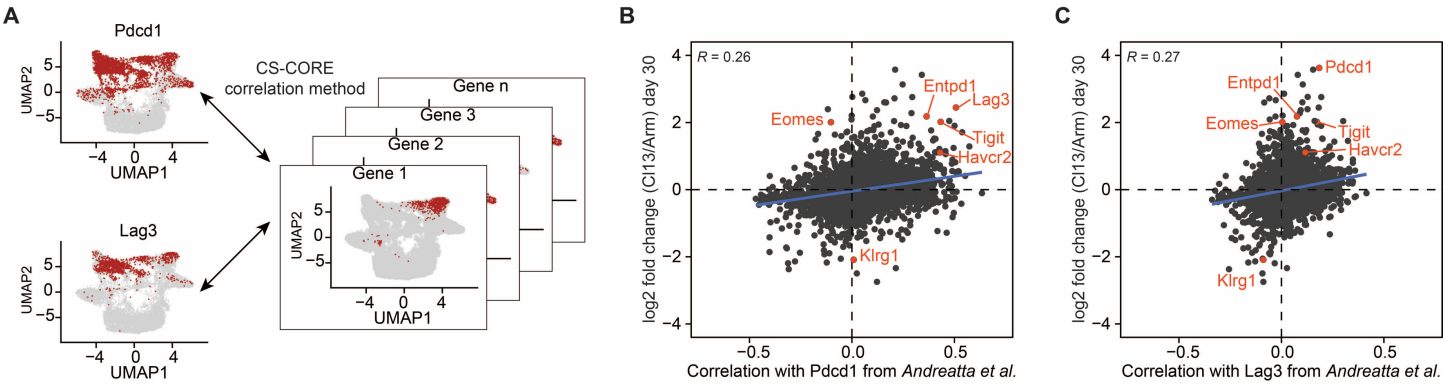

Figure 5: Validation of the proteomic-transcriptional correlation in an orthogonal tumor mouse model. (A) Correlation analysis of single-cell RNA transcriptomics measurements conducted by CS-Core[40]. (**B, C**) Scatter plots illustrating the correlation of genes with PD-1 and Lag3 expression, comparing results from *Andretta et al.*[39], with proteomics measurements. Scatter plot correlation (R) was computed using Spearman correlation.

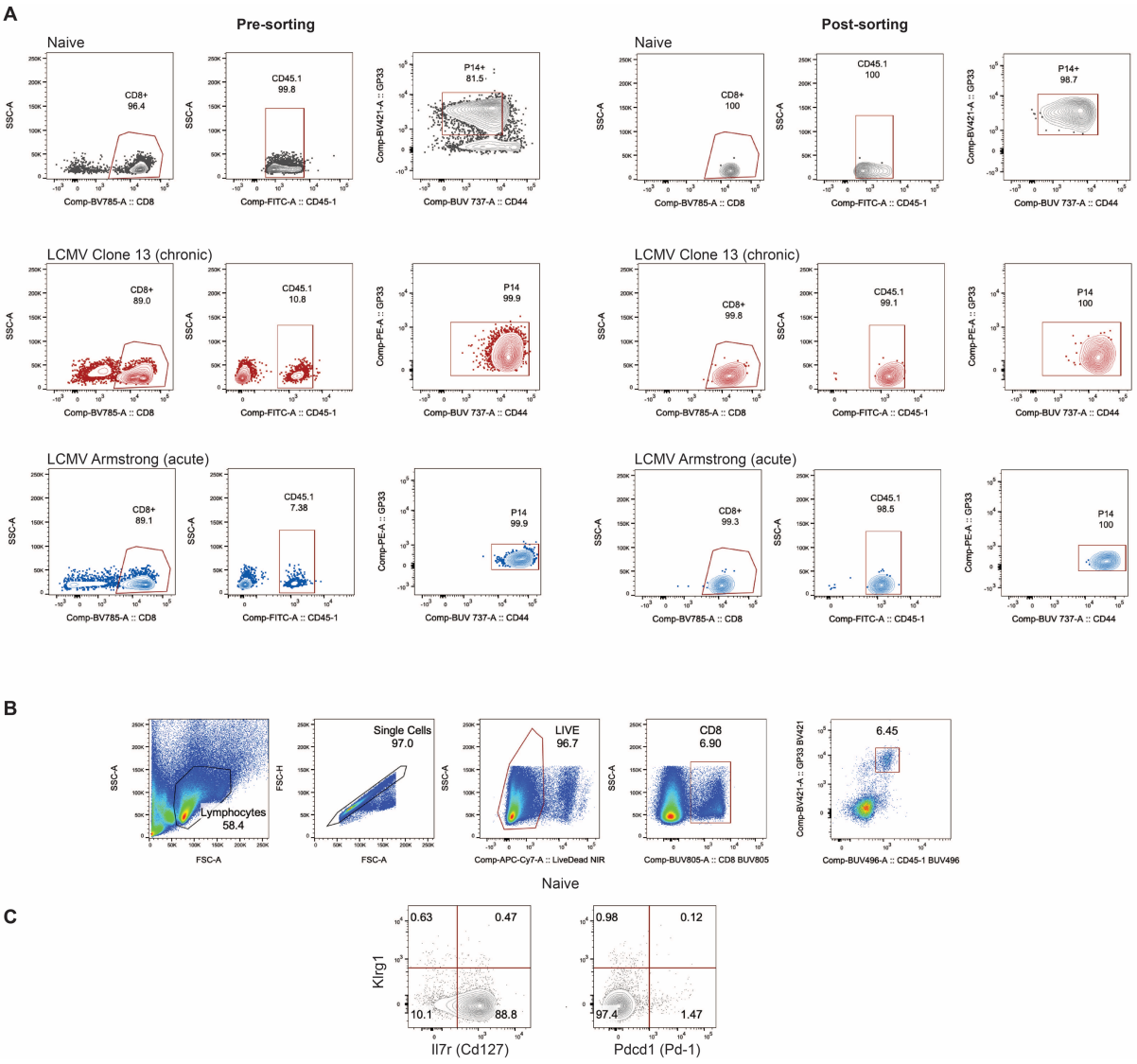

Supplementary Figure S1: Flow cytometry validation of the phenotype and sorting purity of antigen-specific CD8 T cells used for proteomic profiling by MassSpec.

(**A**) Representative dot plots reflecting the sorting purity (post-sorting, right panels) compared to the original frequencies pre-sorting. (**B**) Gating strategy for flow cytometry analysis. (**C**) Representative dot plots of the phenotypic analysis of antigen-specific CD8 T cells.

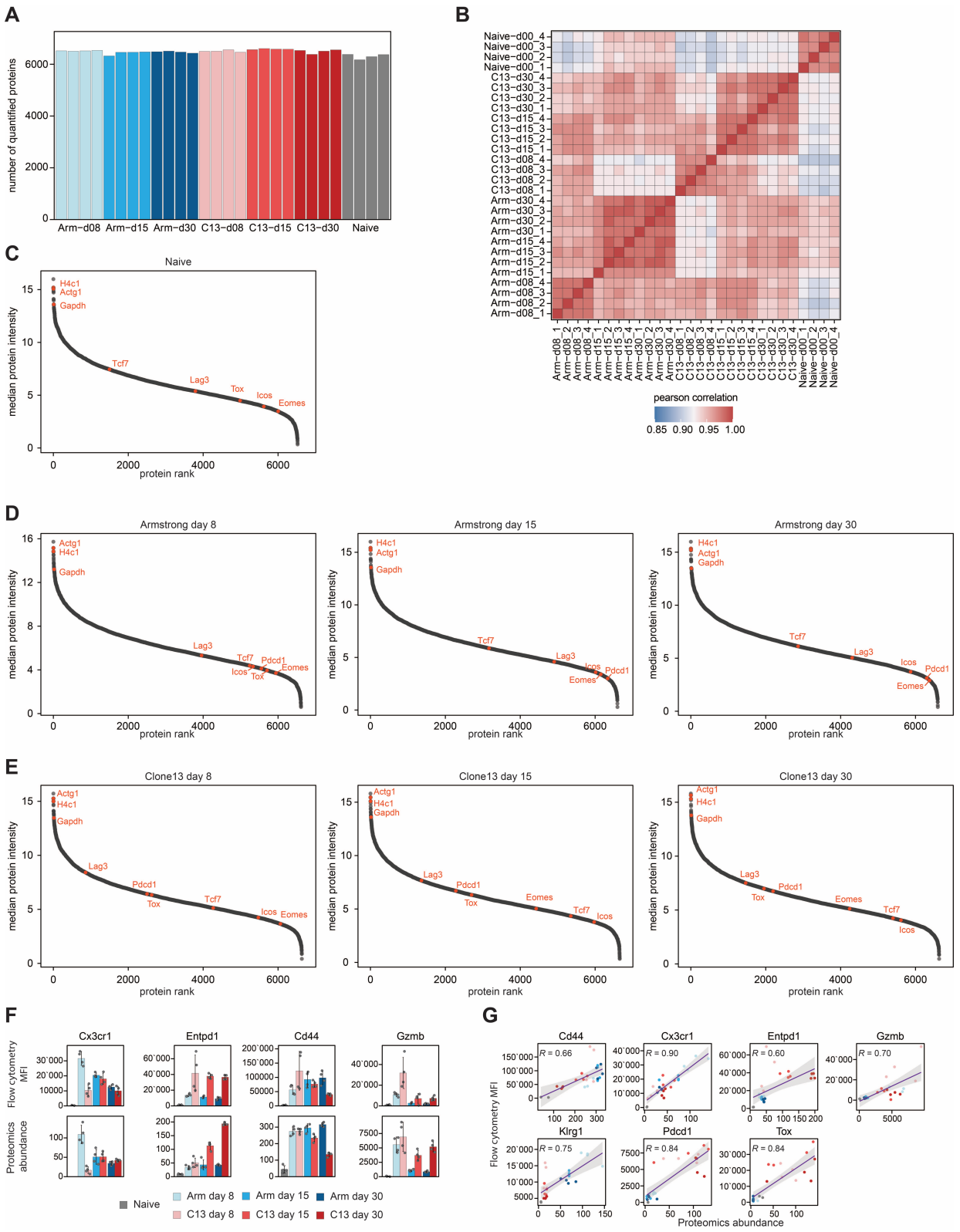

Supplementary Figure S2: Logistics of protein abundance profiling of antigen-specific CD8 T cells in the context of acute and chronic infection. (**A**) Number of quantified proteins in each proteomics sample. (**B**) Correlation between the different samples from all four biological replicates. (**C-E**) Dynamic range for the protein abundance quantification for the naive (**C**), acute (**D**), and chronic (**E**) samples. (**F**) Comparison of protein expression assessed through flow cytometry (top) and proteomics (bottom). The absence of a measurement bar indicates no quantification. (**G**) Correlation (Pearson) between protein expression levels assessed through flow cytometry (Y-axis) and proteomics (X-axis). Naive B6 mice were used as staining controls in (F-G).

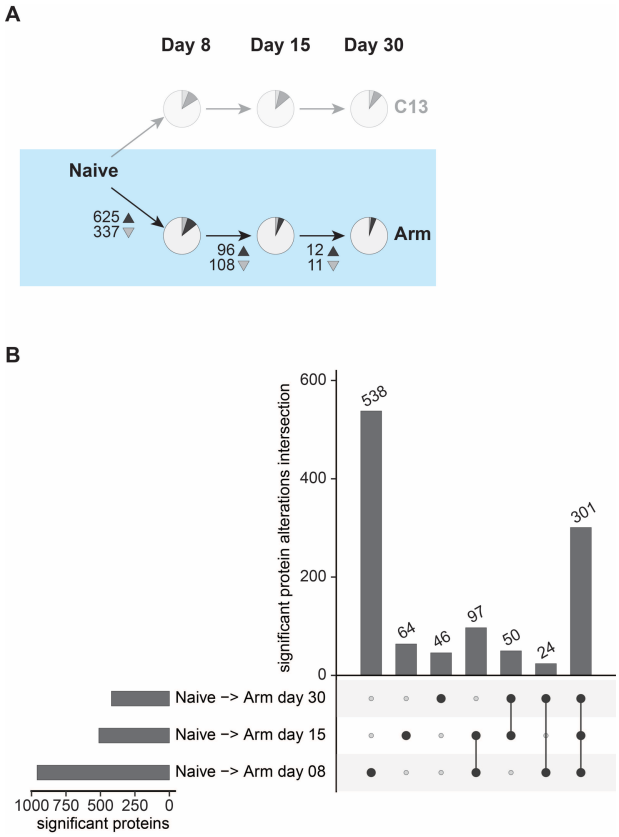

Supplementary Figure S3: Protein abundance alterations associated with T cell differentiation during acute viral infection. (**A**) Quantification of protein abundance alterations across the T cell differential axis in acute LCMV (Arm) infection. (**B**) Significant differentially expressed protein intersections at the different time points post-infection with acute LCMV-Arm compared to naive CD8 T cells ($p < 0.05$ from one-sided ANOVA, absolute $\log_2 FC > 1$).

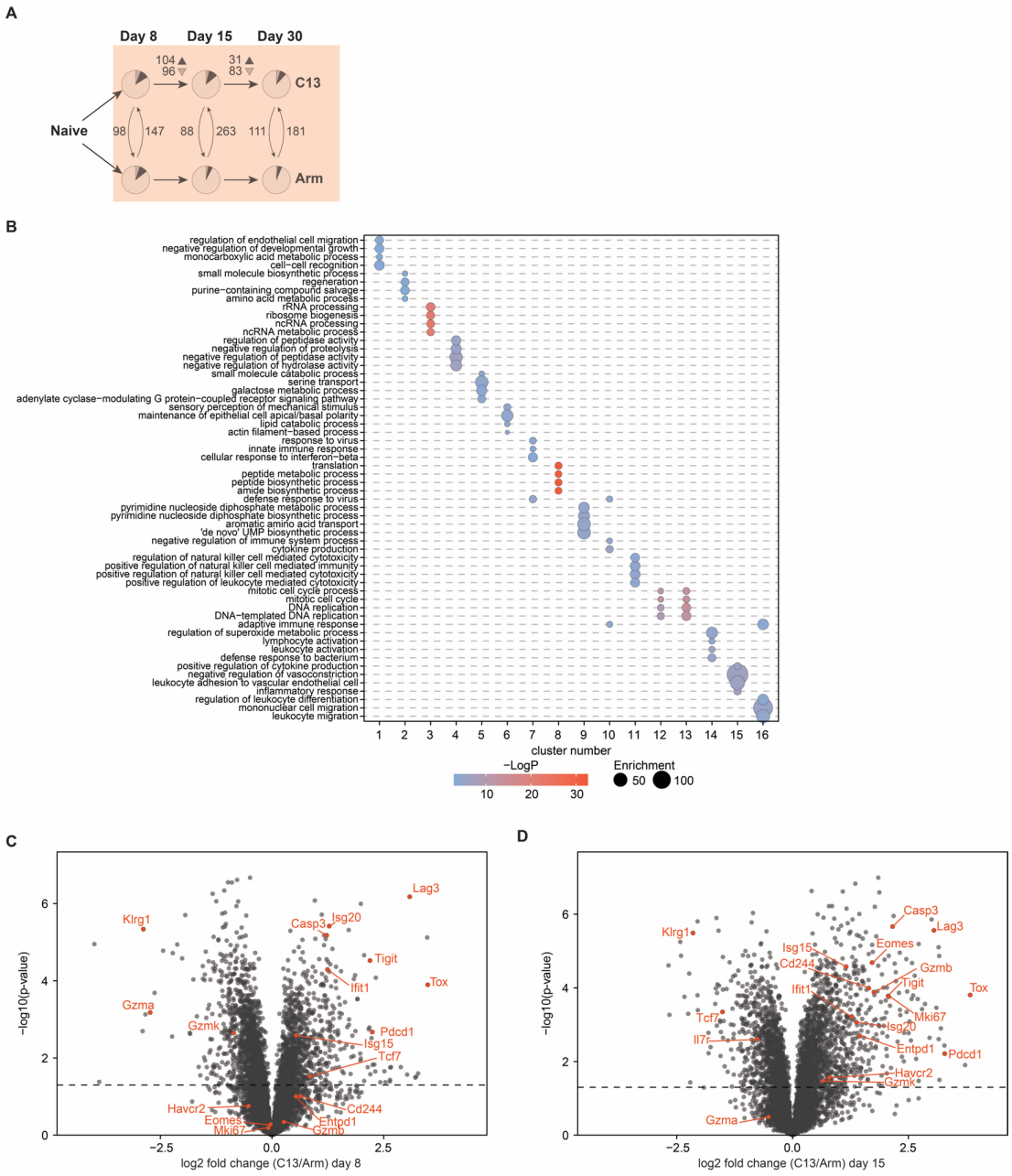

Supplementary Figure S4: Protein alterations in the context of T cell exhaustion compared to differentiation in an acute context. (**A**) Differentially expressed proteins were identified among the highlighted conditions ($p < 0.05$ from one-sided ANOVA, absolute $\log_2FC > 1$). (**B**) Biological processes associated with differentially expressed proteins clustered in Figure 3A and B. (**C-D**) Volcano plots depicting differential protein quantification in CD8 T cells harvested following Armstrong or Clone 13 infection at 8 (**C**) or 15 (**D**) days post-infection.

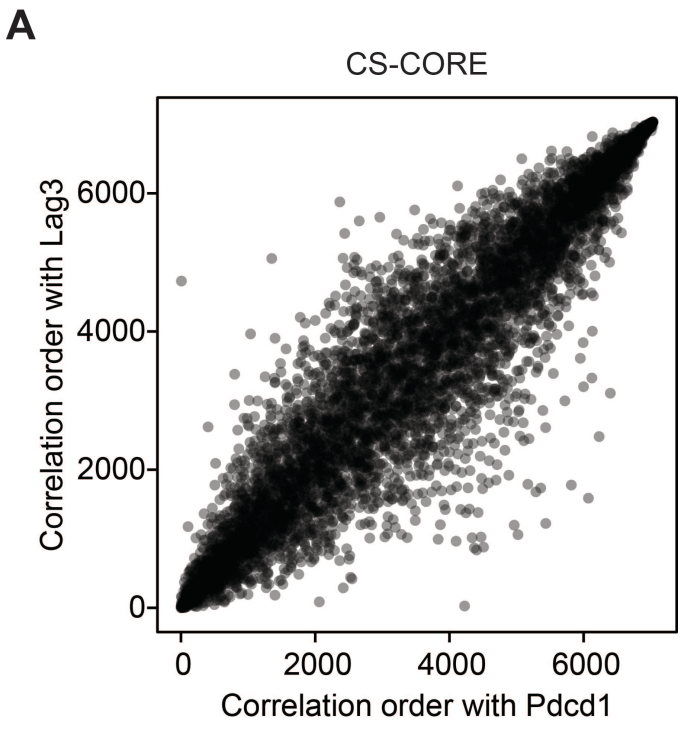

Supplementary Figure S5: Correlation of PD1 and LAG3 gene expression in a mouse tumor model of colon cancer. Correlation of Pdcd1 and Lag3 across scRNAseq data in a mouse colon cancer model.